International Journal of Heat and Mass Transfer 52 (2009) 1112–1122

Contents lists available at ScienceDirect

International Journal of Heat and Mass Transfer

journal homepage: www.elsevier.com/locate/ijhmt

Direct-contact condensation of pure steam on co-current and counter-current stratified liquid flow in a circular pipe

Hyun-Sik Park [a,*], Sung-Won Choi [b], Hee Cheon No [c]

[a] Thermal Hydraulics Safety Research Division, Korea Atomic Energy Research Institute, 1045 Daedeokdaero, Yuseong-gu, Daejeon 305-353, Republic of Korea
[b] School of Nuclear Engineering, Purdue University, 400 Central Drive, West Lafayette, IN 47907, USA
[c] Department of Nuclear and Quantum Engineering, Korea Advanced Institute of Science and Technology, 335 Gwahangno, Yuseong-gu, Daejeon 305-701, Republic of Korea

ARTICLE INFO

Article history:
Received 25 January 2008
Received in revised form 26 August 2008
Available online 4 December 2008

Keywords:
Direct-contact condensation
Co-current flow
Counter-current flow
Heat transfer
Nusselt number

ABSTRACT

We carried out a set of experiments on the direct-contact condensation of atmospheric steam for subcooled water flowing co-currently and counter-currently in a circular pipe. The condensation heat transfer coefficient was evaluated both for co-current and counter-current steam–water flow cases in a horizontal circular pipe. In the current experiment the dependency of the liquid Nusselt number on the gas Reynolds number is higher in the counter-current than in the co-current experimental data. The dependency of the liquid Nusselt number on the steam Reynolds number is stronger in the rectangular channel than in the circular pipe. The overall heat transfer characteristics are better in the co-current flow than in the counter-current flow with the same injection flow rates of the steam and the water. The present co-current experimental data were used to assess four existing correlations. However, there are few reliable correlations existing to predict co-current experimental data. The comparisons of the present counter-current experimental data with the existing correlations show that Chu's (Chu, I.C., Yu, S.O., Chun, M.H. 2000. Interfacial condensation heat transfer for counter-current steam–water stratified flow in a circular pipe, J. Korea Nucl. Soc., 32 (2), 142–156) correlation predicts the experimental data well.

1. Introduction

Direct-contact condensation is a very important thermal–hydraulic phenomenon in LWR (Light Water Reactor) safety analysis and other industrial applications. It could occur in a hot leg during a reflux condensation mode by the water condensed in steam generators with the stratified water, in a cold leg during a postulated LOCA (Loss of Coolant Accident) by the ECC (Emergency Core Cooling) water with the stratified water, and in a downcomer annulus by the injected ECC water with upflow steam flow. Especially the cold ECC (Emergency Core Cooling) water would be injected to cool down the reactor core during a postulated LOCA. When the subcooled water is injected into the horizontal cold leg of a pressurized water reactor filled with steam, the steam flows over the water in the opposite direction and a steam condensation occurs in a stratified flow. The local condensation rate and the relative motion of the steam and water are important in the determination of core uncovery, and the local condensation heat transfer coefficient is one of key parameters of the water hammer because the system behavior is highly dependent upon the local condensation rate. Therefore, experimental data and theoretical analyses are essential for both the co-current and counter-current direct-contact condensation phenomena in a circular pipe and in a rectangular channel together.

There have been a lot of theoretical and experimental researches on a condensation of steam in contact with fairly thick layers of cold water and they were reviewed by Bankoff [1]. Thomas [13] performed an experimental study on the rate at which steam condenses on a pool of turbulent water, under the conditions where a diffusion of heat in a liquid phase is the controlling factor. The measured condensation rate varied strongly with the Reynolds number and a considerable increase in the condensation rate was observed when an agitation of the free surface became sufficiently severe to cause an entrainment of steam bubbles, a condition characterized by the attainment of a critical value of the Kutateladze number. Kim and Bankoff [6] carried out a study of a steam condensation in a counter-current stratified flow steam and subcooled water to measure the local heat transfer coefficient in a rectangular channel inclined 33° in the horizontal direction and the importance of an interfacial shear in enhancing a heat transfer was indicated, and Celata et al. [3] investigated the interaction between saturated or superheated steam in quasi-stagnant conditions and subcooled water in a horizontal flow within a rectangular-duct test section experimentally and developed a laminar-turbulent mathematical model for a macroscopic description of the

* Corresponding author. Tel.: +82 42 868 8615; fax: +82 42 861 6438.
E-mail address: hspark@kaeri.re.kr (H.-S. Park).

0017-9310/$ - see front matter © 2008 Elsevier Ltd. All rights reserved.
doi:10.1016/j.ijheatmasstransfer.2008.08.033

Nomenclature

A	area (m^2)
b	width (m)
c_p	specific heat (J/kg K)
D	diameter (m)
D_h	hydraulic diameter (m)
h	heat transfer coefficient (W/m^2 K)
k	thermal conductivity (W/m K)
Nu	Nusselt number (–)
Pr	Prandtl number (–)
Q	heat flow rate (W)
Re	Reynolds number (–)
S_i	chord length of mass component i (m)
T	temperature (°C)
V	volume (m^3)
W	mass flow rate (kg/s)
y_i	water depth of mass component i (m)

Greek letters

α	void fraction (–)
δ	film thickness (m)
ρ	density (kg/m^3)
μ	viscosity (kg/m^3)
θ	angle (–)
σ	standard deviation (–)

Subscripts

b	bulk, bias limit
c	condensation
ch	rectangular channel
f	liquid
g	gas
in	inlet
log	logarithmic
mean	averaged value along the x axis
out	outlet
P	precision limit
tot	total

phenomenon. Also there have been a lot of theoretical and experimental researches on a horizontal in-channel condensation using a rectangular channel which has a large aspect ratio and a thin water layer thickness. A number of experimental studies (Segev et al. [12], Kim and Bankoff [6], Choi [4]) have investigated an interfacial condensation heat transfer in a stratified co-current steam–water flow in a rectangular channel. However, there are very few experimental data on an in-tube condensation and it is doubtful whether the existing correlations obtained by using a rectangular channel can evaluate the nuclear piping systems of circular pipes directly. Recently Chu et al. [5], Lee et al. [8] investigated an interfacial condensation heat transfer in a stratified smooth and wavy liquid flow in a horizontal pipe, respectively. The importance of the data which is obtained by using the circular pipe, which has a relatively thick water layer, is well discussed by Lee et al. [8]. However, they focused on the counter-current flow of a subcooled thick water layer in a nearly horizontal circular pope with relatively larger inner diameter of 0.084 m. Maron and Sideman [10] theoretically analyzed and compared the vapor condensation rate inside horizontal conduits for co-current and counter-current flow of steam and the accumulated condensate at the bottom of the tube, and [11] investigated the heat transfer by a direct-contact condensation in a stratified two-phase flow at high system pressure and discussed the effect of a thick water layer on the heat transfer characteristics.

The objectives of the present study are to evaluate a condensation heat transfer both in co-current and counter-current flows with a steam–water flow in a horizontal circular pipe. First of all, we investigated the effects of several parameters such as the subcooled inlet water temperature, and the flow rates of the steam and the water. Then, the co-current and counter-current experimental data was also compared with each other and the co-current experimental data in a circular pipe were compared with those in a rectangular channel.

2. Experimental works

2.1. Description of the experimental loop

The overall schematic diagram of the direct-contact condensation experimental facility is shown in Fig. 1. The main components of the experimental facility consist of a water supply system, a steam supply system, the test section and a data acquisition system. The steam supplied by a 100-kW steam generator passes through two steam–water separators and then it is injected into the test section. The steam was purged enough to completely eliminate the non-condensable gas. After the steam temperature reached a saturated steam condition, the steam was purged for more than 1 h, and the generated steam was confirmed to be in a pure steam condition before a test started. The temperature in the steam generator is maintained at about 130 °C during the experiment to compensate for the heat loss in a long pipeline. The flow rate of the steam is controlled by the flow control valve. The inlet water temperature is controlled by a heater and a heat exchanger installed in a water supply tank. The degree of subcooling of the water is controlled based on the temperature measured in the water supply tank. The total length of the horizontal tube is 1.38 m and its inner diameter is 0.06 m.

2.2. Instrumentation

As shown in Fig. 1, several variables are measured to obtain a heat transfer coefficient during direct-contact condensation. The flow rate, the pressure, and the temperature distributions of the mixture layer in the test section are measured locally in the test loop. The inlet pressure and temperature in the test section are measured at the top of the water supply tank connected to the test section.

Fig. 2 shows the schematic diagram of the test section. Inside the test section, the local bulk mean temperatures are measured by using movable thermocouples and the local velocities are measured by using pitot tubes, which are installed at three axial locations. K-type thermocouples with an outer diameter of 0.5 mm are attached to the side of a pitot tube with an outer diameter of 1.5 mm in order to move and measure the local temperature and velocity simultaneously. The level of the water surface is also measured by using a wire conductance probe.

2.3. Test parameters and experimental procedure

The test parameters are selected based on two criteria: one is to estimate the suitability of applying the information obtained by using the rectangular channel system to the pipe system. The other is to examine the effects of several parameters such as the

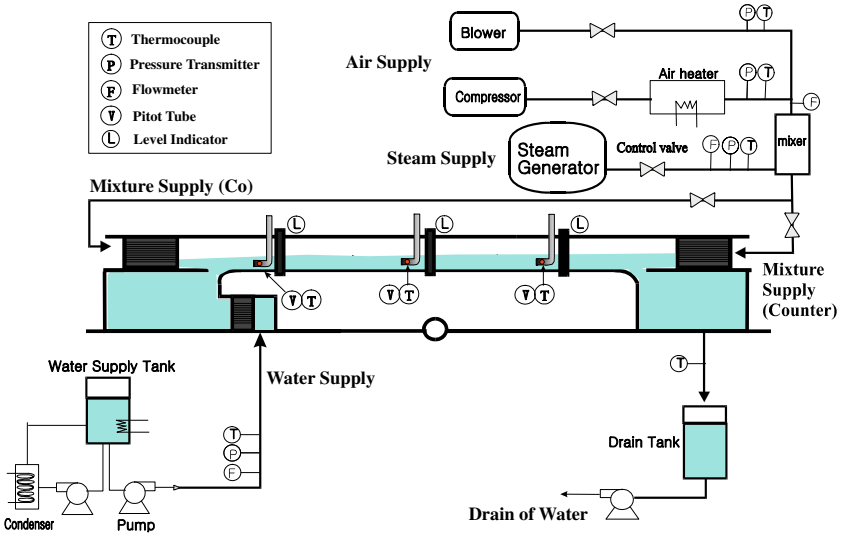

Fig. 1. Schematic diagram of the experimental apparatus.

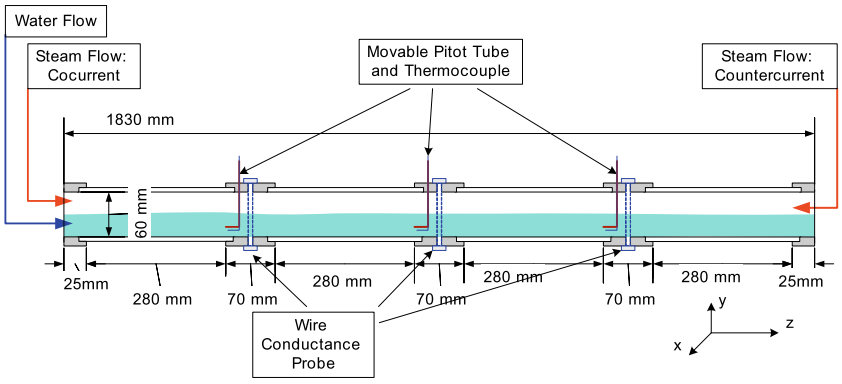

Fig. 2. Schematic diagram of the test section.

subcooled inlet water temperature and the flow rates of the steam and the water. The test parameters considered are the water flow rate, the steam flow rate, the direction of the flow, the inlet water temperature and the inclination angle. The present experimental work is conducted through the following procedure:

(1) Select the flow direction (co-current or counter-current).
(2) Control the inlet water temperature.
(3) Set the inlet water flow rate.
(4) Measure the water layer thickness.
(5) Set the inlet steam flow rate.
(6) Wait until the condition is stabilized to a saturated state.
(7) Measure the vertical temperature and velocity profiles at three axial positions.
(8) Save the data and finish the test.

2.4. Test matrix

The present test matrices are shown in Table 1 for the co-current and counter-current experiments. The control parameters are the inlet flow rates of the water and the steam, and the inlet temperature of the water. The steam in a saturated condition is injected into the test section. The inlet steam temperatures are also

Table 1
Test matrix of the co-current and counter-current experiments.

Test ID	Inlet water temp. (°C)	Inlet steam temp. (°C)	Inlet water flow rate (kg/h)	Inlet steam flow rate (kg/h)
CO001	60.7	100.3	455.1	21.9
CO002	63.8	100.3	450.4	26.6
CO003	63.8	100.5	466.1	39.5
CO004	63.4	100.9	451.3	49.9
CO005	64.1	101.0	438.0	56.9
CO006	60.8	100.3	873.8	20.4
CO007	63.4	100.3	880.4	24.3
CO008	63.4	100.4	876.7	37.3
CO009	63.8	100.5	871.1	47.9
CO010	63.9	100.6	840.2	57.3
CO011	53.6	99.0	1344.2	19.6
CO012	58.0	99.1	1343.3	26.2
CT001	41.1	100.9	297.6	13.3
CT002	41.7	100.9	273.9	21.8
CT003	41.5	100.8	429.7	14.0
CT004	41.9	100.4	447.5	22.5
CT005	41.1	100.8	543.2	13.6
CT006	41.9	100.4	533.9	23.2
CT007	50.9	100.5	305.1	14.0
CT008	52.0	100.7	290.1	21.3
CT009	50.5	100.5	406.5	12.3
CT010	51.2	100.6	406.5	24.2
CT011	49.9	100.5	547.5	13.9
CT012	51.4	100.7	541.9	22.1

listed in Table 1 and the system pressure is at the atmospheric pressure.

For the inclined steam–water co-current flow tests, pure steam condensation tests are performed with an inclination angle of 2.1° and thus the experimental results are comparable to the test results of Choi [4], which used a rectangular channel with a total length of 1.854 m, a width of 0.12 m, and a height of 0.04 m. For the steam–water counter-current flow tests, the test section is slightly inclined (about 0.2° from the water inlet) and thus the experimental condition is comparable to the test cases of Chu et al. [5], which used a circular pipe with a total length of 2.2 m and an inner diameter of 0.084 m.

3. Data reduction method

3.1. Bulk liquid temperature and local liquid mass flow rate

To evaluate the averaged values of the temperature and velocity at each vertical position from the bottom, the temperature and velocity profiles in the cross-sectional horizontal direction are assumed as follows:

(1) The temperature profile is uniform in the cross-sectional horizontal direction, which is experimentally supported from the results of Chu et al. [5].
(2) The velocity profile follows the 1/7 power velocity profile in the cross-sectional horizontal direction.
(3) The properties of the steam along the test section are constant.
(4) The heat transfer from the steam-side and water-side walls to the atmosphere is negligible. Actually the steam condensation rate on the pipe wall is much less than that on the steam–water interfaces.

Additional analyses for a similar geometry (Chu et al. [5]) showed that the velocity profile in the cross-sectional horizontal direction had not only a negligible effect on the bulk water temperature, but also that the bulk water temperature was not changed when with the laminar flow velocity profile was used instead of the 1/7 power velocity profile. The bulk liquid temperature at an axial location is calculated by integrating the measured local data of the vertical velocity and temperature profiles and it is defined as follows:

$$T_{f,b}(z) = \frac{\int \rho_f(x,y,z) V_f(x,y,z) T_f(x,y,z)\, dx\, dy}{\int \rho_f(x,y,z) V_f(x,y,z)\, dx\, dy} \tag{1}$$

In order to evaluate the bulk liquid temperature based on the measured data, the water layer is divided along its height.

Fig. 3 shows the nodalization of the water layer to calculate the water bulk temperature. The water bulk temperature at an axial location is calculated by summarizing the temperatures and velocities at a certain height in the water layer. The liquid bulk temperature can be calculated as follows:

$$T_{f,b}(z) = \frac{\sum_{j=1}^{n} T_{mean}(y_j,z) V_{mean}(y_j,z) S_i(y_j) \Delta y}{\sum_{j=1}^{n} V_{mean}(y_j,z) S_i(y_j) \Delta y} \tag{2}$$

The steam condensation rates at the wall of the test section have been evaluated by a direct measurement of the heat flux in the atmosphere using a micro-foil heat flux sensor and the results showed a negligible wall condensation rate throughout the present tests. Neglecting the condensation rate on the wall and using the relations of the mass and energy conservation for a control volume, the local flow rate of the water can be expressed as

$$W_f(x) = \frac{W_{f,in}(i_g - i_{f,in})}{i_g - i_f(x)} \tag{3}$$

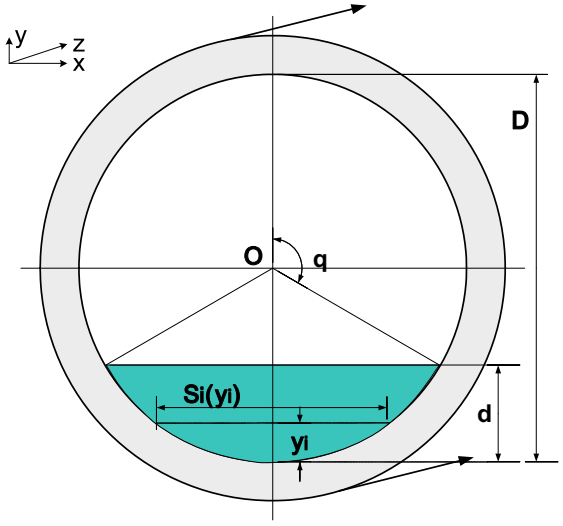

Fig. 3. Nodalization of the calculation of the water bulk temperature.

3.2. Local heat transfer coefficient

The local heat transfer coefficient is calculated by using the gradient of the bulk temperature profile along the flow direction. From the energy balance equation, the local heat transfer coefficient is defined as follow:

$$h_c(z) = \frac{C_{pf} \cdot W_f(z)}{b[T_g - T_l(z)]} \cdot \frac{dT_f(z)}{dz} \tag{4}$$

Since the local mass flow rate, W_f, is also a function of the local liquid temperature, T_f, the local condensation heat transfer coefficient, h_c can be determined only from the local water temperature variations by using the slopes of the liquid temperature, the liquid flow rate, and the temperature difference between phases.

The uncertainty analysis for the local heat transfer coefficients has been carried out by an error propagation method [2]. The independent parameters include the water layer thickness, the inlet water flow rate, the inlet steam flow rate, the local water velocity, and the local bulk temperatures of the steam and the water. The standard deviation of the local heat transfer coefficients σ_h is computed by the root-sum-square method for a bias limit σ_b and a precision limit σ_p as follows:

$$\sigma_h = \sqrt{\sigma_b^2 + \sigma_p^2} \tag{5}$$

The maximum standard deviation of the interfacial condensation heat transfer coefficients is 27.5%, which is mainly due to an error in the water bulk temperature that results from an error which is produced during the determination of the water layer thickness. The detailed information is summarized in Table 2.

Table 2
Uncertainty of the local heat transfer coefficient.

Parameter		Precision limit	Bias limit
Independent parameter	Water layer thickness (m)	0.005	0.001
	Inlet water flow rate (%)	2	1
	Inlet steam flow rate (%)	5	1
	Local water velocity (%)	5	5
	Local water and steam temperature (°C)	0.5	1.2
Local heat transfer coefficient, h (%)		24.4	12.8
Maximum standard deviation of local heat transfer coefficient, σ_h (%)		27.5	

3.3. Log-mean heat transfer coefficient

The log-mean heat transfer coefficient can be obtained from the total heat transfer rate, heat transfer area and the measured liquid and steam temperatures both at the inlet and outlet as follows:

$$h_{\log} = \frac{Q_{tot}}{A \cdot \Delta T_{\log}} \tag{6}$$

where A is the total heat transfer area, $\Delta T_{\log}$ the log mean temperature difference, and Q_{tot} the total heat flux from the inlet to the outlet. The log-mean temperature difference is defined by

$$\Delta T_{\log} = \frac{\Delta T_1 - \Delta T_2}{\ln(\Delta T_1 / \Delta T_2)} \tag{7}$$

where $\Delta T_1 = T_{g,in} - T_{f,in}$ and $\Delta T_2 = T_{g,out} - T_{f,out}$.Here, $T_{g,in}$, $T_{g,out}$, $T_{f,in}$, and $T_{f,out}$ are the mean temperatures of the gas and the liquid both at the inlet and outlet, respectively.

3.4. Dimensionless numbers

The dimensionless parameters used in the present work are the condensation Nusselt number, the Reynolds numbers, and the Prandtl number. The liquid Nusselt number is defined as

$$Nu_f = \frac{h \cdot D_{h,f}}{k_f} \tag{8}$$

The Reynolds numbers of the liquid and the gas are

$$Re_f = \frac{\rho_f V_f D_{h,f}}{\mu_f} \text{ and} \tag{9}$$

$$Re_g = \frac{\rho_g V_g D_{h,g}}{\mu_g}, \tag{10}$$

and the liquid Prandtl number is

$$\Pr = \frac{c_{p,f}\mu_f}{k_f,}, \tag{11}$$

Where

$$D_{h,f} = \frac{\pi D \cdot \alpha_f}{\pi - a + \sin\theta} \tag{12}$$

$$D_{h,g} = \frac{\pi D \cdot \alpha_g}{a + \sin\theta}, \text{ and} \tag{13}$$

$$a = \pi\alpha_g + \cos\theta \cdot \sqrt{1 - \cos^2\theta} \tag{14}$$

4. Test results and discussions

4.1. Flow regime

The experimental data are plotted on Mandhane et al.'s [9] flow pattern map to identify the flow regimes of the co-current and counter-current gas–liquid flows in a horizontal pipe as shown in Fig. 4. While the present experimental conditions of a co-current flow lie in the wavy flow region and some data lies in the region very close to the boundary between the wavy flow and the slug flow, the present experimental conditions of the counter-current flow lie in the stratified flow region and on the interface between the stratified and wavy flow regions. Their predictions of the flow regimes are identical with the visual observations. As shown in Fig. 4, the superficial velocities of the steam and liquid were higher in the co-current test cases than in the counter-current test cases. The water layer thicknesses were from 8.1 to 17.2 mm and from 17.6 to 22.6 mm for the co-current and counter-current tests, respectively.

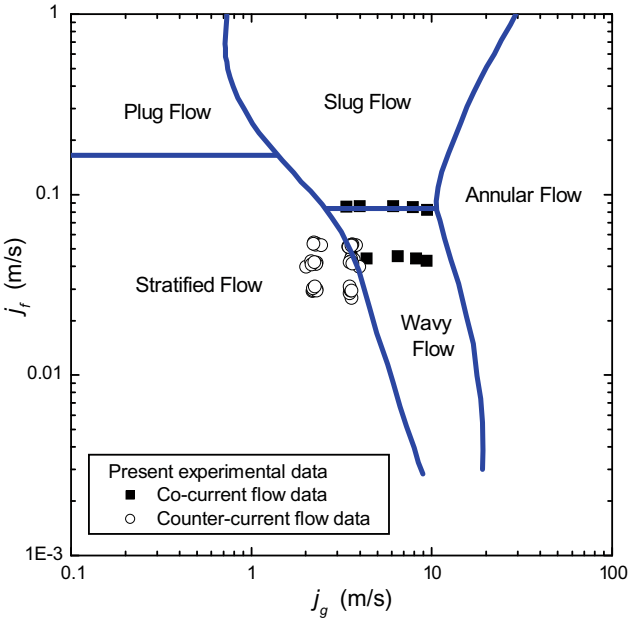

Fig. 4. Experimental data plotted on the Mandhane et al.'s [9] flow pattern map.

4.2. Local water temperature and velocity

Figs. 5 and 6 show the typical profiles of the local water temperature and the local water velocity measured at the three locations of 0.441, 0.895, and 1.349 m downstream from the water inlet. The typical test case of the co-current condensation experiment is CO003. The inlet water temperature was 63 °C, and the inlet Reynolds numbers of the water and the steam are 13,516 and 19,341, respectively. As shown in Fig. 5(a), the liquid region can be classified into three regions in the vertical direction; the water layer close to the bottom (bottom region), the water layer close to the steam–water interface (interface region) and the in-between (transition region). For the case of CO003, in the bottom region ($y^* < 0.8$) the local water temperature remains constant. The local liquid temperature increases along the flow direction in the bottom region, while it converges to a constant temperature in the transition region ($0.8 < y^* < 0.9$) and then it rises sharply to the saturation temperature in the interface region ($y^* > 0.9$). The regional boundaries are changed by the initial and boundary conditions. As shown in Fig. 6(a), the local velocities of the water layer increase from the bottom region to reach their highest velocities at the end of the transition region and then they decrease through the interface region.

The typical test case of the co-current condensation experiment is CT001. The inlet water temperature was 41 °C, and the inlet Reynolds numbers of the water and steam were 3994 and 6823, respectively. Similar to the co-current test cases, the liquid region in Fig. 5(b) can be classified into three regions of bottom, interface and transition. For the case of CT001, in the bottom region ($y^* < 0.6$) the local water temperature remains constant. The local water temperatures are almost constant along the flow direction in the bottom layer, while they increase along the flow direction in the transition region ($0.6 < y^* < 0.8$) and then they rise sharply to the saturation temperature in the interface region ($y^* > 0.8$). The regional boundaries between the bottom and transition regions and between the transition and interface regions are deeper in the counter-current cases than in the co-current cases. The temperature distribution in the counter-current flow is different from that in the co-current flow. The water bulk temperature in the bottom region is almost constant, which implies that condensation occurs

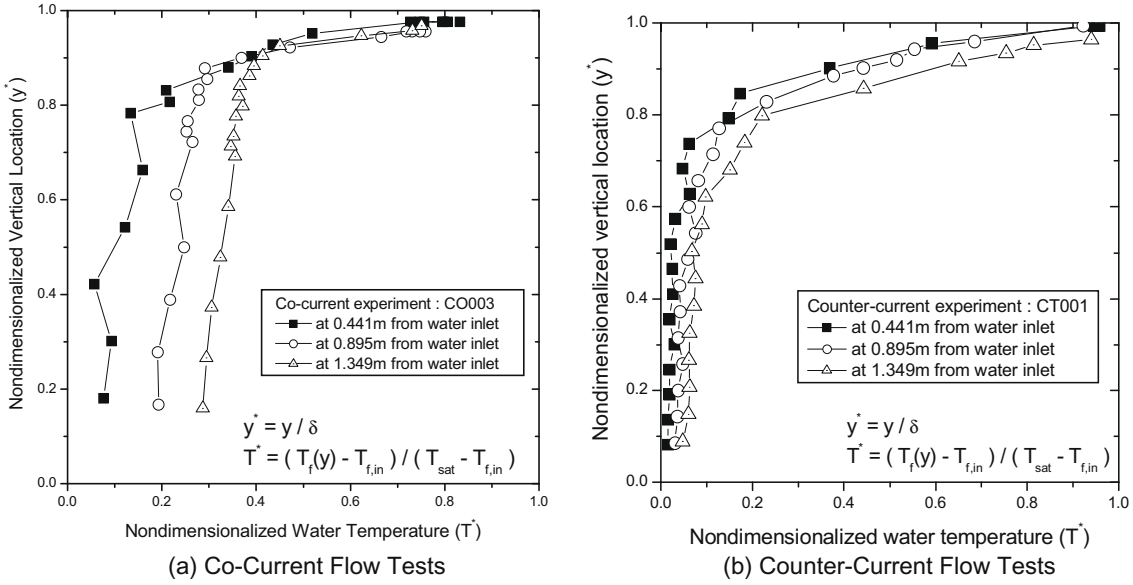

Fig. 5. Profiles of the local water temperature for the co-current and counter-current flow tests.

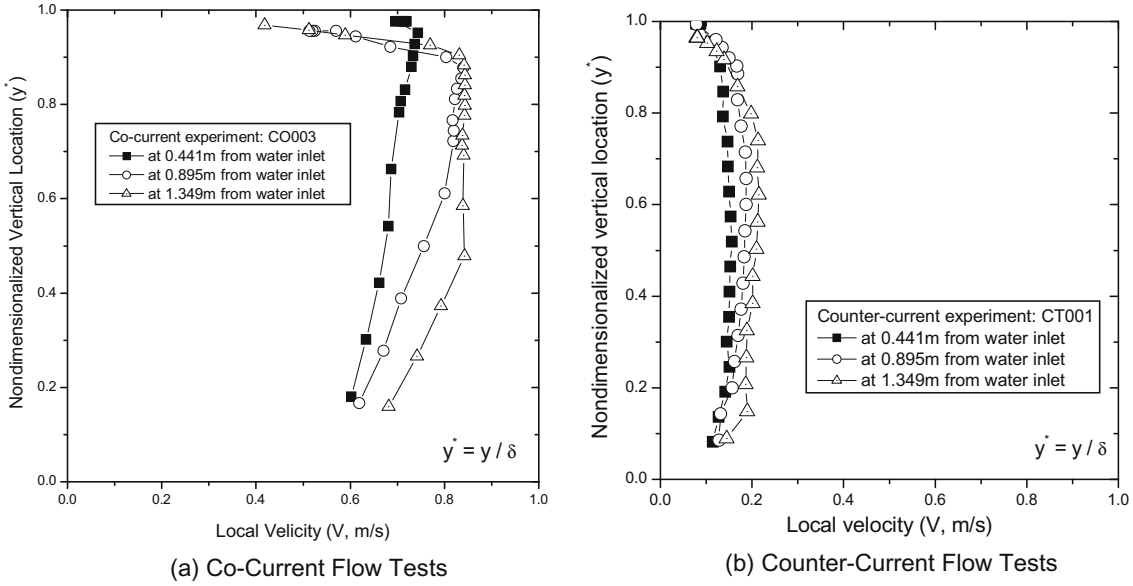

Fig. 6. Profiles of the local water velocity for the co-current and counter-current flow tests.

in the steam–water interface region and it does not affect the bottom region. The affected interface region becomes wider due to the counter-current motion of the steam and the liquid and their mixing. As shown in Fig. 6(b), the local velocities of the water layer increase from the bottom region to reach their highest velocities at the transition region and then they decrease through the interface region. The velocity distribution is different from that in the co-current flow. The velocity profile in the counter-current flow is flatter along the vertical direction than that in the co-current flow and its maximum velocity is located at around $y^* = 0.8$.

4.3. Logarithmic heat transfer coefficient and nusselt number

We perform 24 sets of co-current and counter-current condensation experiments using pure steam. Logarithmic heat transfer coefficients are calculated for the pure steam data. Fig. 7 shows the effects of the inlet steam and liquid Reynolds numbers on the logarithmic heat transfer coefficients. Fig. 7(a) is for the co-current flow tests. The logarithmic heat transfer coefficient is plotted against the inlet steam Reynolds number, in which the inlet liquid Reynolds number is used as a parameter. The logarithmic heat transfer coefficient increases with an increase in the inlet steam Reynolds number and it also increases slightly with an increase in the inlet liquid Reynolds number. Fig. 7(b) is for the counter-current flow tests and the inlet steam Reynolds number is used as a parameter. The results were similar to the experimental results of the co-current flow tests.

Fig. 8 shows the effects of the inlet steam and liquid Reynolds numbers on the logarithmic Nusselt numbers. Fig. 8(a) is for the co-current flow tests. The logarithmic Nusselt number is plotted against the inlet steam Reynolds number, in which the inlet liquid Reynolds number is used as a parameter. The tendency of the logarithmic Nusselt number is similar to that of the logarithmic heat transfer coefficient. However, the dependency of the Nusselt num-

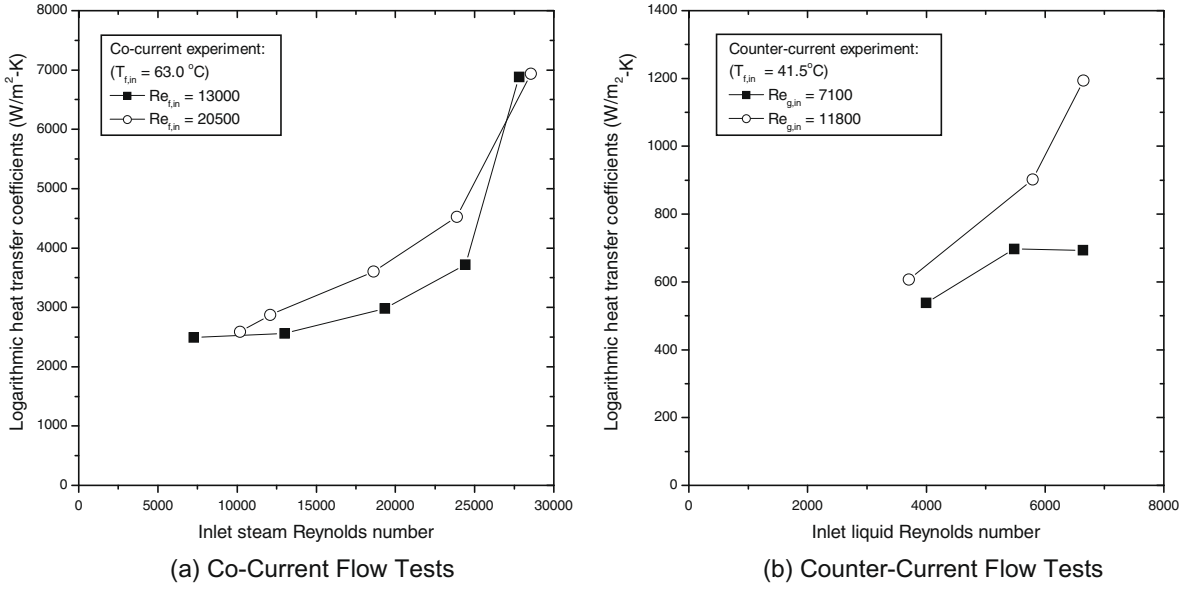

Fig. 7. Effects of the inlet steam and liquid Reynolds numbers on the logarithmic heat transfer coefficient.

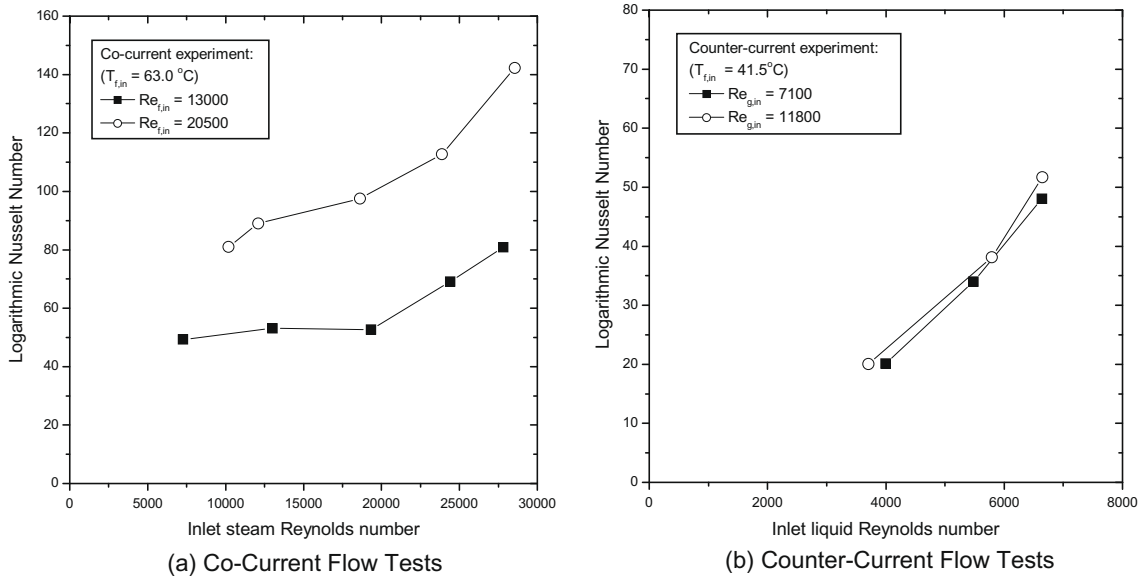

Fig. 8. Effects of the inlet steam and liquid Reynolds numbers on the logarithmic Nusselt number.

ber on the inlet liquid Reynolds number is stronger than that of the heat transfer coefficient. Fig. 8(b) is for the counter-current flow tests. The dependency of the logarithmic Nusselt number on the inlet steam Reynolds number is weaker when compared with that of the logarithmic heat transfer coefficient, which is due to the fact that the higher steam flow makes the film thickness thinner.

4.4. Local liquid nusselt number

Fig. 9 shows the effect of the inlet liquid Reynolds number on the local liquid Nusselt number. Fig. 9(a) is for the co-current flow tests, which have a similar inlet steam Reynolds number of 13,000. The local liquid Nusselt number decreases along the flow direction of both the steam and water. It is higher with a higher inlet liquid Reynolds number. Fig. 9(b) is for the counter-current flow tests, which have a similar inlet steam Reynolds number of 11,800. The results were similar to the experimental results of the co-current flow tests.

Fig. 10 shows the effect of the inlet steam Reynolds number on the local liquid Nusselt number. Fig. 10(a) is for the co-current flow tests, which have a similar inlet water Reynolds number of 20,500. The local Nusselt number decreases along the flow direction. It is higher with a higher inlet steam Reynolds number. The local liquid Nusselt number is similar around the water inlet but it decreases rapidly along the flow direction. With an increased inlet steam Reynolds number its decreasing rate becomes slower. Fig. 10(b) is for the counter-current flow tests, which have similar inlet water Reynolds numbers of 4893 and 6348. The results were similar to the experimental results of the co-current flow tests.

4.5. Assessment of the previous correlations

The experimental results show that the liquid Nusselt number becomes much higher with an increased liquid Reynolds number. However, its dependency on the gas Reynolds number is very small. Fig. 11 shows the comparison of the Nusselt

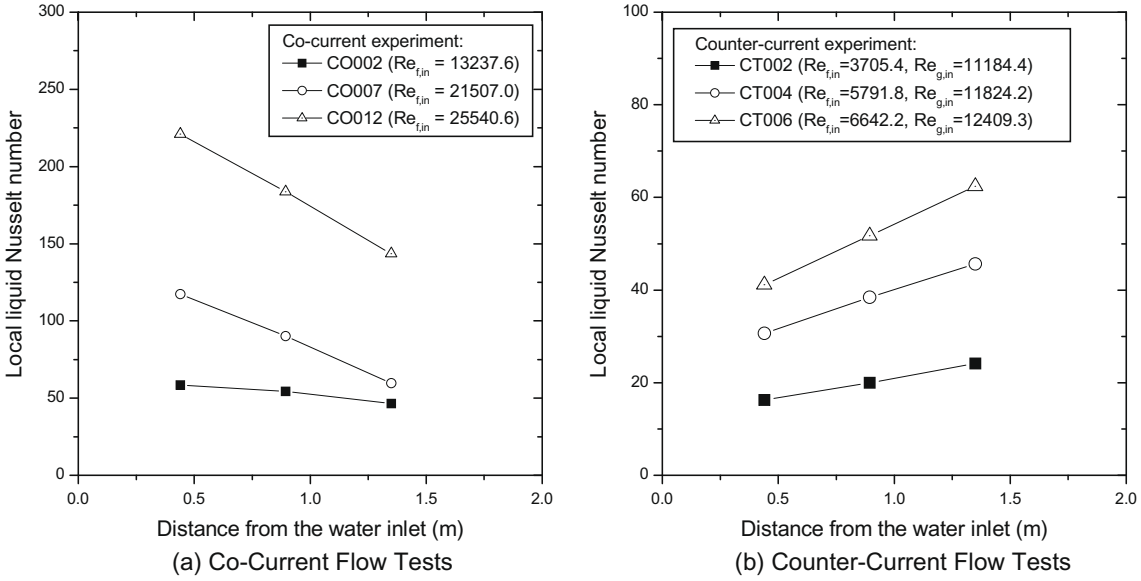

Fig. 9. Effect of the inlet liquid Reynolds number on the local liquid Nusselt number.

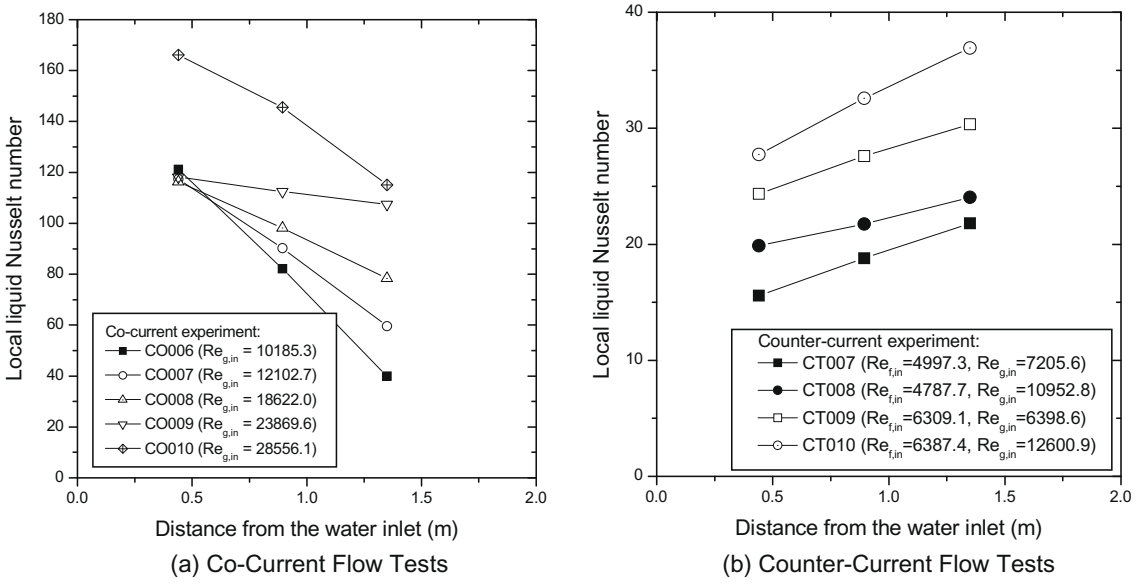

Fig. 10. Effect of the inlet steam Reynolds number on the local liquid Nusselt number.

numbers estimated from the co-current and counter-current experimental data with those calculated from four existing correlations. Table 3 shows test sections and heat transfer correlations for the direct-contact condensation, which are used for the assessment of the present experimental data. Fig. 11(a) is for the co-current experimental data. Kim and Bankoff's [6] correlation with the Froude number overestimates the experimental Nusselt numbers with a standard deviation of 153.4%, and the other three correlations of Chu et al. [5], Segev et al. [12], Kim and Bankoff's [6] with the Reynolds number, deviate with standard deviations of 47.6%, 38.0%, and 40.2%, respectively. The above correlations are developed based on counter-current experimental data and they can not well predict the present co-current experimental data. Furthermore, there are no reliable existing correlations based on co-current condensation data. It is concluded that there is a need to develop a correlation for co-current condensation phenomena to be generally applicable to both a rectangular channel and pipe geometry. Fig. 11(b) is for the counter-current experimental data. Kim and Bankoff's [6] correlation with the Froude number overestimates the experimental Nusselt numbers with a standard deviation of 132.5%, and the other three correlations of Chu et al. [5], Segev et al. [12], Kim and Bankoff's [6]) with the Reynolds number, deviate with standard deviations of 15.6%, 29.7%, and 31.7%, respectively. The correlations obtained by Segev et al. [12], Kim and Bankoff [6]) are based on a rectangular flow channel and a very shallow water layer thickness. However, the correlation obtained by Chu et al. [5] is based on the experimental data obtained by using a circular pipe with a diameter of 0.084 m and its predictions over the present experimental data are comparatively accurate. The results show that the direct application of the data or correlations acquired with the rectangular channel geometry to the pipe geometry can cause an inaccurate prediction of the condensation phenomena.

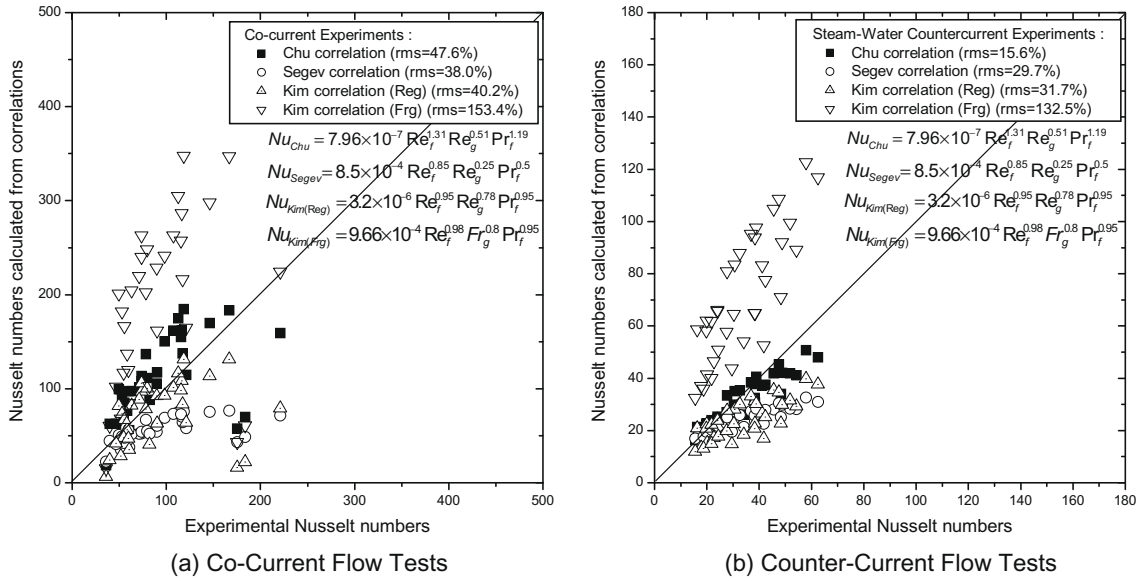

Fig. 11. Comparison of the local Nusselt numbers between the circular tube and rectangular channel data.

Table 3
Comparison of test sections and heat transfer correlations for the direct-contact condensation.

Author	Cross section and inclination (degree from the horizontal)	Dimension (m)	Flow direction	Heat transfer correlations
Chu et al. [5]	Circular and 0°	I.D. = 0.084 Length = 2.20	Counter-current	$Nu = 7.96 \times 10^{-7} Re_f^{1.31} Re_g^{0.51} Pr_f^{1.19}$
Segev et al. [12]	Rectangular and 17°, 45°	Width = 0.152 Height = 0.051 Length = 1.066	Counter-current	$Nu = 8.5 \times 10^{-4} Re_f^{0.85} Re_g^{0.25} Pr_f^{0.5}$
Kim et al. [7]	Rectangular and 4°, 30°, 33°, 87°	Width = 0.38 Height = 0.075,0.038 Length = 1.27	Counter-current	$Nu = 3.2 \times 10^{-6} Re_f^{0.95} Re_g^{0.78} Pr_f^{0.95} Nu = 9.66 \times 10^{-4} Re_f^{0.98} Fr_g^{0.8} Pr_f^{0.95}$
Present work	Circular and 0°	I.D. = 0.06 Length = 1.38	Co- and counter-current	–

4.6. Comparison of the heat transfer characteristics between the co-current and counter-current flows

The test cases of CO001 and CT010 are selected to compare the heat transfer characteristics between the co-current and counter-current flow cases. It should be noted that the degrees of the inclination angle of both the co-current and counter-current condensation experiments are 2.1° and about 0.3° (slightly inclined), respectively. Figs. 12 and 13 show the comparisons of the local heat transfer coefficient and Nusselt number, respectively, between the co-current and counter-current flows. The local values are also higher in the co-current flow than in the counter-current flow. The local heat transfer coefficient and Nusselt number are higher at the steam inlet for both the co-current and counter-current flow cases. Although the inlet flow rates are similar, the Reynolds numbers are different because the film thickness and thus its hydraulic diameter have different values. The water layer is thinner in the co-current case than in the counter-current case. It is caused by the higher inclination angle and the sweeping of the water by the co-current steam. The liquid hydraulic diameter in the co-current case of CO001 is about half of that in the counter-current case of CT010. Thus the influence region of the heat transfer through the water layer is deeper and the liquid-side heat transfer rate is higher in the co-current case than in the counter-current case, which can be understood through the comparison of the temperature profiles of Fig. 5. In the bottom layer the local temperature is changed more along the flow direction in the co-current case than in the counter-current case. As further work both effects should be clarified with data with the same inclination angle. Although the heat transfer rate is increased by the higher relative velocities and the higher interface roughness in the counter-current case than in the co-current case, the effect of the thinner water layer on the overall heat transfer rate is higher.

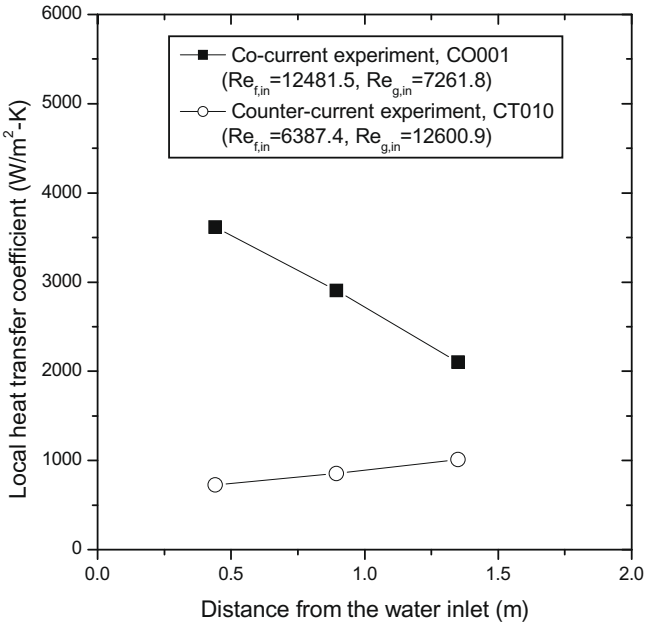

Fig. 12. Comparison of the local heat transfer coefficient between the co-current and counter-current flow tests.

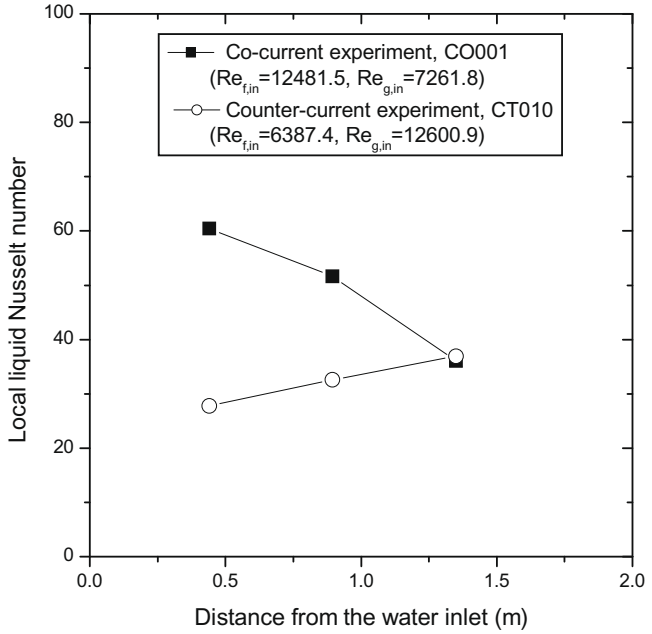

Fig. 13. Comparison of the local Nusselt number between the co-current and counter-current flow tests.

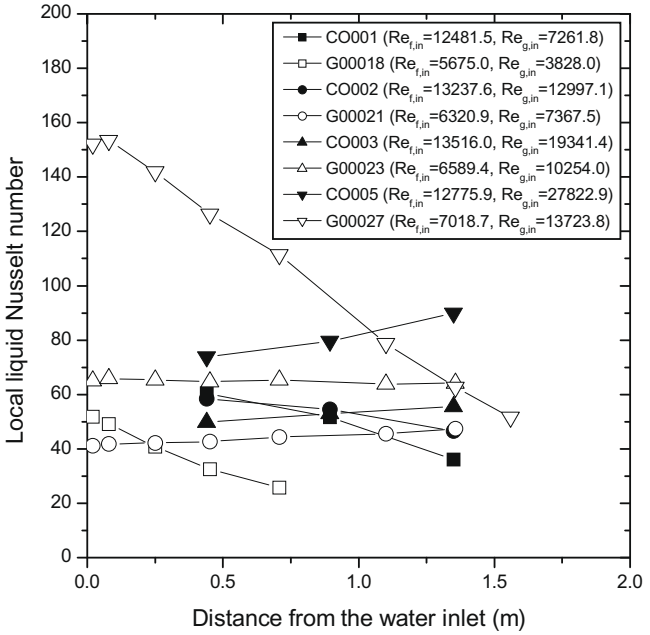

Fig. 14. Comparison of the Nusselt numbers estimated from the experimental data with those calculated from the existing correlations.

The logarithmic heat transfer coefficients of CO001 and CT010 are 2493 and 1066 W/m^2 *K*, respectively, and the logarithmic Nusselt numbers of CO001 and CT010 are 49.3 and 32.3, respectively. The overall heat transfer characteristics are better in the co-current flow than in the counter-current flow with the same injection flow rates of the steam and the water. These experimental data seem to experimentally verify Maron and Sideman's [10] theoretical finding experimentally, which shows that the co-current flow is the recommended mode of operation when the higher condensate production rate is desired at given temperature driving force for given tube length.

4.7. Comparison with the rectangular channel data

The co-current experimental data was compared with the rectangular channel data of Choi [4] whose test section was made with a rectangular channel. The hydraulic diameter of the rectangular channel was 0.06 m, which is the same diameter as that of the present circular pipe. Fig. 14 shows a comparison of the local Nusselt numbers between the circular tube and rectangular channel data.

The comparable data was selected from the database of the rectangular channel condensation experiment. In this study the experimental data with the inclination angle of 2.1° was used to compare the heat transfer characteristics of the circular pipe and the rectangular channel data. The selected test cases are G00018, G00021, G00023, and G00027, which can be compared with the present test cases of CO001, CO002, CO003, and CO005, respectively.

The Reynolds numbers of the liquid and the gas for the rectangular channel are

$$Re_{f,ch} = \frac{\rho_f V_f \delta_f}{\mu_f} \text{ and} \tag{15}$$

$$Re_{g,ch} = \frac{\rho_g V_g \delta_g}{\mu_g}, \tag{16}$$

and the Nusselt number for the rectangular channel is defined as

$$Nu_{f,ch} = \frac{h \cdot \delta_f}{k_f}, \tag{17}$$

As the hydraulic diameter of the rectangular channel is approximately two times that of the liquid film thickness, the comparable Reynolds numbers and liquid Nusselt number of the circular pipe are approximately two times those of the rectangular channel.

The inlet liquid Reynolds number is similar to each other for all the cases but the inlet steam Reynolds number is varied considerably. For the low inlet steam Reynolds number, the local liquid Nusselt numbers of the circular pipe are higher than those of the rectangular channel, while for the high inlet steam Reynolds number, the local liquid Nusselt numbers of the circular pipe become lower than those of the rectangular channel. The water layer is less affected by the flowing steam as the water layer in the circular pipe is thicker than that in the rectangular channel. The dependency of the liquid Nusselt number on the steam Reynolds number is weaker in the circular pipe than in the rectangular channel.

5. Conclusions

Several experiments were performed to obtain reliable data on the interfacial condensation phenomena for both the co-current and counter-current flows in a horizontal circular pipe. The parametric effects on the condensation heat transfer were investigated and the experimental data was used to assess the existing correlations. Also the co-current condensation data was compared with the rectangular channel data and the co-current and counter-current data was compared with each other. From the aforementioned studies, the following conclusions have been reached:

(1) For both the co-current and counter-current flow tests the logarithmic heat transfer coefficient and Nusselt number increase as both the inlet liquid and steam Reynolds numbers increase.
(2) A comparison of the co-current experimental data with the existing correlations shows that there are no reliable correlations to accurately predict the co-current experimental data, and thus there is a need to develop a new model to predict both a circular pipe and rectangular channel data.

(3) The present counter-current experimental data was also used to assess the existing correlations. Comparisons of the present experimental data of the counter-current flow with four existing correlations showed that [5]'s correlation is the best among the selected four correlations.
(4) The dependency of the liquid Nusselt number on the gas Reynolds number is higher in the counter-current than in the co-current experimental data. This tendency is also shown in the axial distribution of the local Nusselt number. The overall heat transfer characteristics are better in the co-current flow than in the counter-current flow with the same injection flow rates of the steam and the water.
(5) The dependency of the liquid Nusselt number on the steam Reynolds number is stronger in the rectangular channel than in the circular pipe.

References

[1] S.G. Bankoff, Some condensation studies pertinent to LWR safety, Int. J. Multiphase Flow 6 (1980) 51–67.
[2] P.R. Bevington, Data Reduction and Error Analysis for the Physical Science, McGraw Hill, Inc., New York, NY, USA, 1969.
[3] G.P. Celata, M. Cumo, F. D'Annibale, G.E. Farello, G. Focardi, A theoretical and experimental study of direct contact condensation on water in turbulent flow, Exp. Heat Transfer 2 (1989) 129–148.
[4] Choi, K.Y., 1998. Direct-contact Condensation Heat Transfer with Noncondensable Gases and Interfacial Shear for Co-current Stratified Wavy Flow in Nearly-Horizontal Channels, Ph.D. Thesis, KAIST, Daejeon, Korea.
[5] I.C. Chu, S.O. Yu, M.H. Chun, Interfacial condensation heat transfer for countercurrent steam–water stratified flow in a circular pipe, J. Korea Nucl. Soc. 32 (2) (2000) 142–156.
[6] H.J. Kim, S.G. Bankoff, Local heat transfer coefficients for condensation in stratified countercurrent steam–water flows, J. Heat Transfer, Trans. ASME 105 (1983) 706–712.
[7] H.J. Kim, S.C. Lee, S.G. Bankoff, Heat transfer and interfacial drag in countercurrent steam–water stratified flow, Int. J. Multiphase Flow 11 (1985) 593–606.
[8] K.W. Lee, I.C. Chu, S.O. Yu, H.C. NO, Interfacial condensation for countercurrent steam–water stratified wavy flow in a horizontal circular pipe, Int. J. Heat Mass Transfer 49 (2006) 3121–3129.
[9] J.M. Mandhane, G.A. Gregory, K. Aziz, A flow pattern map for gas–liquid flow in horizontal pipes, Int. J. Multiphase Flow 1 (1974) 537–553.
[10] D.M. Maron, S. Sideman, Condensation inside near horizontal tubes in co-current and counter-current flow, Int. J. Heat Mass Transfer 25 (9) (1982) 1439–1444.
[11] Ruile, H., 1995. Heat transfer by direct contact condensation in stratified two phase flow at high system pressure. In: Two-Phase Flow Modeling and Experimentation, Rome, Italy, pp. 269–276.
[12] A. Segev, L.J. Flanigan, R.E. Kurth, R.P. Collier, Experimental study of counter-current steam condensation, J. Heat Transfer, Trans. ASME 103 (1981) 307–311.
[13] R.M. Thomas, Condensation of steam on water in turbulent motion, Int. J. Multiphase Flow 5 (1979) 1–15.